Local Zoom Computation of Two-Phase Flows in Steam Generators using a Local Defect Correction Method

Michel Belliard, Marc Grandotto

▶ **To cite this version:**

Michel Belliard, Marc Grandotto. Local Zoom Computation of Two-Phase Flows in Steam Generators using a Local Defect Correction Method. Numerical Heat Transfer, Part A, 2003, 43 (2), pp.111-135. hal-00274330

HAL Id: hal-00274330
https://hal.science/hal-00274330

Submitted on 21 Apr 2008

HAL is a multi-disciplinary open access archive for the deposit and dissemination of scientific research documents, whether they are published or not. The documents may come from teaching and research institutions in France or abroad, or from public or private research centers.

L'archive ouverte pluridisciplinaire **HAL**, est destinée au dépôt et à la diffusion de documents scientifiques de niveau recherche, publiés ou non, émanant des établissements d'enseignement et de recherche français ou étrangers, des laboratoires publics ou privés.

LOCAL ZOOM COMPUTATION OF TWO-PHASE FLOWS IN STEAM GENERATORS USING A LOCAL DEFECT CORRECTION METHOD

M. Belliard[1] and M. Grandotto

Commissariat à l'Energie Atomique (CEA)

DRN/DTP/STH/LMTA

C.E. CADARACHE, 13108 Saint Paul-lez-Durance Cedex, France

A Local Defect Method used to perform local zoom computations within the framework of the steady state two-phase flow simulations of PWR Reactors Steam Generators is described. The particular LDC formulation used, jointly with the FEM, a projection algorithm and the Crank-Nicholson scheme for non-linear averaged mixture balance equations, is discussed, as well as the particular geometry involved (3D local hierarchical multigrid). In the case of vortices located at an inner interface, the boundary conditions are dynamically managed in a approach 'à la Adaptive Dirichlet Neumann'. Cluster workstations, using a master-slaves context (through a code-linker) and the PVM package, are used. Results concerning the simulation of a mock-up are provided. The parallel and sequential LDC computation results are compared with the results of classical full domain computations. The conclusion describes the improvements in the accuracy of the corrected region and on the coherence between the zoom and the full domain.

Nomenclature

Latin symbols

- a: Schlichting model dimensionless constant
- A: subset of M_1 coarse nodes included in D_2

[1]e-mail : michel.belliard@cea.fr

- $\mathring{A}$: subset of internal nodes of A
- B_i: boundary nodes of mesh M_i
- cp: coupling period
- D_1: global domain (whole computation domain)
- D_2: zoom domain
- $\overrightarrow{g}$: gravity (m s^{-2})
- $\overrightarrow{G}$: mixture mass flux ($= \rho \overrightarrow{v}$)
- H: mixture specific enthalpy (J kg^{-1})
- H_{ls}: saturated liquid specific enthalpy (J kg^{-1})
- k: coupling iteration counter
- L: latent heat (J kg^{-1})
- L_v: typical vortex length (m)
- M_1: global domain mesh (coarse)
- M_2: zoom domain mesh (fine)
- n: outer iteration (or pseudo time step) counter
- P: pressure (Pa)
- Q: heat source (W m^{-3})
- t: time (s)
- T_p: primary fluid temperature (K)

- $\overrightarrow{v}$: mixture velocity (m s^{-1})
- $\overrightarrow{v_R}$: relative velocity (gas minus liquid, m s^{-1})
- x: static quality ($\equiv \frac{H-H_{ls}}{L}$)

Grrek symbols

- α: relaxation parameter
- β: porosity ($=\Omega_m/\Omega$)
- χ_T: turbulent diffusion coefficient for the energy equation (kg m^{-1} s^{-1})
- φ^i: nodal function
- $\bar{\Lambda}$: two-phase friction tensor (s^{-1})
- μ_T: two-phase turbulent dynamic viscosity (N s m^{-2})
- Ω: elementary volume (m^3)
- Ω_m: mixture volume (m^3)
- ρ: mixture density (kg m^{-3})
- ζ: generic imposed boundary value

1 INTRODUCTION

An application of a Local Zoom method, the Local Defect Correction (LDC, [1]) method, is presented, in the context of 3D two-phase flow computations. Our application is the simulation of French nuclear steam generator (SG) risers where liquid water boils, see Fig. 1. Simulations are needed to evaluate SG performances and perform a safety analysis. The difficulties reside

in the differences in geometrical and physical scales, turbulent and 3D flows through complex internal structures, exchanges between the two phases,..

In an industrial background, the problem is simplified by a gas-liquid mixture approach, as in the GENEPI software (in French: "GENErateur Programme Industriel") [2, 3, 4]. However, the amount of data to store for each control volume limits the spatial resolution. In particular, this problem is crucial when high spatial resolution is needed in only some parts of the SG. On the one hand, a fine mesh for the full domain is too expensive and unnecessary. On the other hand, locally increasing the space discretization is not easy with the numerical method used, especially a standard Finite Elements Method. Our goal is to:

- locally increase the simulation accuracy (without the computation at high resolution of the whole domain),
- deal with non-conforming grids through the use of two grids in a local hierarchical multigrid (MG) context,
- deal with flow vortices at the boundaries of the zoom region,
- deal with simulations of zoom regions fully embedded in the global domain,
- increase the simulation possibilities: increase the memory and reduce the CPU time,

by using a memory distributed parallel implementation of local zoom methods on cluster workstations.

The LDC method is used jointly with a dynamic determination of the boundary conditions in order to face the presence of flow vortices at the interfaces of the zoom region. This approach is similar to the treatment of the boundary conditions in the Adaptive Dirichlet Neumann method (ADN) [5] in a Domain Decomposition context. Hence, we call it ("à la ADN").

This paper is structured as follows. The second part is dedicated to a brief presentation of the

two-phase flow model and to the numerical aspects. The coupling strategy is emphasized in the third part. In the fourth one, the Local Defect Correction method used for the zoom computations in a 3D local hierarchical multigrid context and the dynamic management of the boundary conditions are presented. Finally, numerical results concerning some zoom simulations of the U-tube bundle and of the flow distribution baffle regions of a SG Mock-up are given in the fifth part.

2 TWO-PHASE FLOW MODEL

After averaging the mass, momentum and energy equations for each phase [6], these are merged to obtain a mixture description of the two-phase flow. Provided that the following assumptions hold: (i) surface tension, viscous and turbulent dissipation are neglected and pressure terms are neglected in the enthalpy balance equation, (ii) same pressure for steam and liquid, (iii) eddy viscosity model, one obtains:

1. mass balance

$$\beta\partial_t\rho + \overrightarrow{\nabla}.(\beta\rho\overrightarrow{v}) = 0 \tag{1}$$

2. momentum balance

$$\begin{aligned}&\beta\rho\partial_t\overrightarrow{v} + \beta\rho(\overrightarrow{v}.\overrightarrow{\nabla})\overrightarrow{v} + div(\beta x(1-x)\rho\overrightarrow{v_R}\otimes\overrightarrow{v_R})\\ &= \beta\rho\overrightarrow{g} - \beta\bar{\Lambda}\rho\overrightarrow{v} - \beta\overrightarrow{\nabla}P + div(\beta\mu_T(\overrightarrow{\nabla}\overrightarrow{v} + \overrightarrow{\nabla^t}\overrightarrow{v}))\end{aligned} \tag{2}$$

3. enthalpy balance

$$\beta\rho\partial_t H + \beta\rho(\overrightarrow{v}.\overrightarrow{\nabla})H + div(\beta x(1-x)\rho L\overrightarrow{v_R}) = \beta Q + div(\beta\chi_T\overrightarrow{\nabla}H) \tag{3}$$

We solve in H, P and $\overrightarrow{v}$ variables. (Even if we solve in $\overrightarrow{v}$, it is the $\overrightarrow{G}$ variable that plays the more important role due to the mass balance equation, see below.) In order to compute ρ, x and L in function of H and P, we need water thermodynamic tables. The μ_T, χ_T, $\bar{\Lambda}$, $\overrightarrow{v_R}$ terms are obtained by the use of a large set of semi-empirical closure relations [4]. The most often used are the Schlichting model for μ_T ($\mu_T = a|\overrightarrow{G}|L_v$ where a is a dimensionless constant and L_v a typical vortex length, [7]) and the drift-flux Lellouche-Zolotar model [8], based on the Zuber-Findlay approach [9], for $\overrightarrow{v_R}$. The heat source Q in the enthalpy equation is linked to the resolution of an energy balance equation for the primary flow. To evaluate this term, other correlations on the heat exchange coefficient and the wall temperature are included.

According to the hyperbolic nature of the flow equations, Dirichlet boundary conditions are used at the inlets of the domain (mass flux and enthalpy) and Neumann boundary conditions at the outlets (pressure). The other boundaries of the domain are impermeable walls. Generally, these are considered adiabatic and with no shear stress (the strong pressure drop induced by the tube bundle leads us to neglect the wall shear stress).

3 NUMERICAL CONSIDERATIONS

The stationary flow is approached with a pseudo-transient computation. According to this computational approach, a steady-state problem is solved by performing pseudo-time steps. Moreover, in our applications, the wave effects can be neglected (linked to the time term in the mass balance equation). In fact, the time term is eliminated in Eq. (1). By doing this, an incompressible flow simulation is mimicked, substituting the free divergence equation ($div\,\overrightarrow{v} = 0$) by a similar one involving the mass flux ($div\,\overrightarrow{G} = 0$). This allows us to use the powerful Chorin-Gresho method [10] to simultaneously solve the couple ($\overrightarrow{G}$,P). The numerical scheme is based on the unstructured finite element method (FEM) with tri-linear hexahedral elements and a Crank-Nicholson time

scheme. The H and $\overrightarrow{v}$ variables take values at the nodes. In contrast, the P variable is defined as constant per element. Concerning the equation coefficients (x, ρ, $\overrightarrow{v_R}$, ...), these are generally defined per element, except for β which is a nodal field. The stress and thermal flux terms are integrated by parts. The lumping of the mass matrix [11] is done and *one point integration* is used to compute the element matrices. The diffusive terms are implicit as is the frictional one (momentum). Generally, the advective and drift terms are explicit. Like Gresho and al., we include a balancing tensor diffusivity (BTD) correction to increase the stability of the central difference advection scheme [12]. At each pseudo-time step ($\equiv$ outer iteration to solve non-linear coupled equations), we first solve the primary fluid energy equation (fully implicit FEM) to obtain the enthalpy source term Q. Thus, the enthalpy equation is solved and then the coupled mass-momentum ones are solved by the Chorin-Gresho method.

A conjugated gradient method (CGM) ($\equiv$ inner iterations), preconditioned by the diagonal, is used to solve the arising linear systems.

4 THE COUPLING STRATEGY

Based on the master/slave concept, we have developed a general application [13] with the CEA code-linker software called ISAS [14] which uses the PVM software. In this application, several GENEPI tasks run together, coupled at every *cp* (a given coupling period) outer iterations - or pseudo-time iterations - by the ISAS task. Thus, a Multiple Instructions Multiple Data (MIMD) application, with distributed memory, on a workstation network is mimicked. The pseudo-time step is independent in each task (stationary flow simulation).

For each GENEPI task, the user can set up some 'coupled boundaries'. Each coupled boundary is defined by a boundary condition type (such as Dirichlet, ADN, LDC, ...), a GENEPI task name (providing the data) and an operator name (such as interpolation, restriction, ...).

When dealing with conforming meshes, linear interpolations or direct affectations of fields on the coupled boundaries are performed. In case of non-conforming meshes, only linear interpolations can be performed.

To increase stability and convergence, a relaxation process is introduced on the values (flux and variables) imposed on the coupled boundaries. We denote α the relaxation parameter:

$$\zeta^k = \alpha\zeta^* + (1-\alpha)\zeta^{k-1} \tag{4}$$

Here, ζ stands for the imposed boundary values, k for the current coupling iteration and ζ^* for a new value coming from an external task.

After some information exchanges, here through the ISAS Master task, each GENEPI slave task knows what data it needs and what data it must provide at each coupling iteration (external requests). Concerning the coupling process, each coupling iteration is done in three steps.

- Each task sends messages to the master in order to supply data for its external requests.
- Each task receives data, from the master, for its own coupled boundaries.
- Each task runs *cp* outer iterations (i.e. pseudo-time steps).

And the process is run again for the next coupling iteration. At the end of the *cp* outer iterations, the convergence test is run for the slaves and the result is sent to the master. If all the slaves have reached the convergence, then the master stops them. The convergence test includes convergence tests for the variables (H, P and $\vec{G}$) and for the coupled boundary values (H, $\vec{G}$, thermal flux and mechanical stress).

Two strategies are available. In the first one (additive version), the coupling iterations are run together. Then, the slaves process the data coming from the previous coupling iteration, as in a Jacobi process. In the second one (multiplicative version), after the first step (send data),

some slaves are put to sleep during a full coupling iteration: the second and third steps of the current one and the first step of the next one. Then the slaves are awoken to receive data and run *cp* outer iterations. With this approach, the slaves process the newest available data as in a Gauss-Seidel process.

5 LOCAL ZOOM COMPUTATION

We want to perform the computation of a local subdomain with a fine mesh and, at the same time, use this high resolution information to increase the accuracy of the simulation of the whole domain. To do this, we use local hierarchical meshes (local multigrid) and the Local Defect Correction method.

5.1 The Local Defect Correction method

5.1.1 Overview

We want to reach a steady state flow simulation using a transient computation. Consequently, there are time terms in the balance equations (or similarly terms coming from a relaxation process). The used semi-implicit approach leads to a splitting of the equation terms into an operator part (left-hand side, implicit) and a source part (right-hand side, explicit). Moreover, the source terms in the balance equations are dependent on the variables. But, in fact, the mean purpose of this pseudo-time scheme is to overcome the non-linearity (the relaxation process already mentioned).

In the introduced LDC application, the time terms are not taken into account, the focus being only on the steady state equations to solve. Hence, we prefer to take into account equations with the following form:

$$T(u) = 0 \quad with\ BC. \tag{5}$$

The goal of the LDC method is to locally correct the discretized operator, say T_i, involved in the numerical resolution of a discretized equation on a given mesh M_i:

$$T_i(u_i) = 0 \quad with\ BC. \tag{6}$$

For a fixed discretization order, the error here comes from the space discretization (space step). Basically, we deal with two discretizations of the operator T (associated in the FEM context with two given meshes). A coarse one (or standard one, T_1) in the whole computation domain, say M_1, and a fine one, T_2, in the zoom region (improvement in the space step), say M_2. Generally, the coarse discretization allows an easy numerical resolution, but may introduce large errors in some specific parts of the computation domain. Contrarily, the numerical resolution is better with the fine discretization, but more expensive. Hence, we may only compute part of the whole domain: the zoom region. The strategy is to solve the local problem with the better discretization and locally correct the standard expression of the operator in the whole domain. To do this, an iterative process is used.

For a detailed presentation of the LDC method, see Hackbusch's original paper [1]. It is worth pointing out that the LDC method allows a general framework to locally correct the global domain computation using a local improved approximation coming from a more precise computation scheme that may completely differ from the global domain scheme: finite volume method, spectral method,... In the following section, the modified LDC method used in the GENEPI software is presented, including the non-linearity.

5.1.2 The application of the LDC method in GENEPI

Let M_1 be the mesh associated with the standard space discretization of the global domain D_1 and M_2 the mesh associated with the local problem on the zoom domain D_2 (better discretization).

And let B_1 be the boundary of M_1 and B_2 be the boundary of M_2. The local mesh and the global mesh are embedded forming a hierarchical grid structure. The internal boundary is given by $B_2 \backslash (B_1 \cap B_2)$. Let A be the coarse nodes of the M_1 mesh included in the zoom region D_2 and $\mathring{A}$ be the internal nodes of A.

The iterative process is the following. Let χ be the characteristic function of $\mathring{A}$ and u_1^0 the initial approximation of the solution on the mesh M_1.

- start with $f_1^0 = 0$,
- given f_1^k, $k = 0, 1, 2, ...$
  - do some smoothing iterations for the global problem $T_1(u_1^k) = f_1^k$ on M_1,
  - compute the internal boundary values on M_2, by interpolation for instance,
  - do some smoothing iterations for the local problem $T_2(u_2^k) = 0$ on M_2,
  - compute the restriction of u_2^k (called $ru2_1^k$) on nodes of A (in M_1),
  - define the next right-hand side by: $f_1^{k+1} = \chi\, T_1(ru2_1^k)$.

We add the LDC terms to the right-hand parts of the secondary flow energy balance equation and momentum balance equation. No correction is performed on the mass balance equation (free divergence of the mass flux, see below). Here, u_j^k stands for the couple (H, Q) for the energy balance equation and for ($\overrightarrow{G}$, P) for the momentum balance equation. The LDC term is kept constant during a coupling iteration (in fact during several pseudo-time steps). This term involved in the modified right-hand side of the equation is similar to a multigrid correction (MGC) term. Basically, this algorithm may be viewed as a classical LDC iteration loop in which the local and global problems are not solved exactly, but only a few iterations *cp* of one iterative method are performed: the usual numerical techniques of GENEPI, namely outer iterations for the non-linearity (transient computation with a semi-implicit approach) and a Conjugated

Gradient type method for the linear system solving. It can be viewed in terms of classical outer iterations (i.e. pseudo-time iterations) with periodic updates of the defect correction values for the global problem and of the boundary values for the local one. Concerning the global problem, the defect correction is added to the constant source term of the balance equation's RHS. Hence, the introduction of a constant term does not introduce modifications of the Chorin algorithm based on Taylor's development in time. So, the pressure equation is unchanged.

We have presented the multiplicative version (sequential) of the algorithm, but we have also developed an additive version (parallel). In all cases, one slave GENEPI task runs for the global domain computation and several others for the zoom subdomain computations (one per subdomain). Data are sent from the zoom subdomain to the global one for the purpose of filling the defect correction values. Depending on the type of balance equation, the sent data are specific enthalpy, mass flux, volume thermal source or pressure. Then, by means of canonical restrictions (for the nodal variables, here denoted u):

$$u_1 = u_2 \tag{7}$$

or volume V weighted restrictions (for the thermal sources and pressures, here denoted Q):

$$V_1 Q_1 = \sum_e Q_2^e V_2^e \tag{8}$$

we restrict these data on all nodes or cells of the global domain mesh included in the zoom region A (but not at the B_1 Dirichlet nodes). The local defect correction values are computed for the nodes of the global mesh included in the correction region, $\mathring{A}$. Theses nodes, included in A, are distant from the internal boundary nodes by more than one or two elements (in the first case, the coarse corrected nodes do not lie in the coarse elements bordering the internal boundary).

The extension of this region is managed by the code users.

5.1.3 The correcting term for the energy balance equation

Let us come back to the correcting term described in Section 5.1.2 and symbolically denoted by $T_1(ru2_1)^i$. Here, $ru2_1$ stands for the restriction, at the nodes of subset A (see Section 5.1.2) of the global domain, of the mixture specific enthalpy (notation : Hr), of the mixture pressure (notation : Pr) and of the mixture mass flux (notation : $\overrightarrow{Gr}$) initially computed on the zoom subdomain. In the same way, $T_1(...)^i$ stands for the integral of the energy balance equation (written with all terms in the LHS) weighted by the nodal function associated at the node i: φ^i. Hence, the counterpart of the symbolic operator $T_1(ru2_1)^i$ is the finite element formulation of the following term (in case of the drift flux hypothesis), on the mesh of the global domain :

$$T_1(ru2_1)^i \equiv \int \overrightarrow{dX}\varphi^i[\beta(\overrightarrow{Gr}.\overrightarrow{\nabla})Hr + div(\beta x_r(1-x_r)\rho_r L_r \overrightarrow{v_{Rr}})] \\ - \int \overrightarrow{dX}\varphi^i \beta Q_r + \int \overrightarrow{dX}[(\overrightarrow{\nabla}\varphi^i)(\beta\chi_T \overrightarrow{\nabla} Hr)] + BC \qquad (9)$$

with $L_r(Pr)$ latent heat, $x_r(Hr, Pr)$ static quality, $\rho_r(Hr, Pr)$ mixture density, $\overrightarrow{v_{Rr}}(Hr, \overrightarrow{Gr}, Pr)$ relative velocity, Q_r source term, including the restricted volume thermal source, the boundary thermal flux and, eventually, the pressure gradient terms. If it exists, this last term is a function of the restricted variables (Hr, $\overrightarrow{Gr}$, Pr). Concerning the non-linearity, the weakness lies in the values of χ_T, computed with the variables taken at the current outer iteration (i.e. pseudo-time iteration), and in the values of the volume thermal source (use of the restricted volume thermal source instead of the exact computation with Hr, $\overrightarrow{Gr}$ and Pr). It is to be noted that this correction term is no more than the energy balance equation weighted residual.

5.1.4 The correcting term for the momentum balance equation

The correcting term $\overrightarrow{T_1}(ru2_1)^i$ at node i, with the same previously defined restricted variables, is the finite element formulation of the following expression (in case of the drift flux hypothesis) :

$$\begin{aligned}\overrightarrow{T_1}(ru2_1)^i \equiv & \int \overrightarrow{dX}\varphi^i[\beta(\overrightarrow{Gr}.\overrightarrow{\nabla})\overrightarrow{vr} + div(\beta x_r(1-x_r)\rho_r\overrightarrow{v_{Rr}}\otimes\overrightarrow{v_{Rr}})] \\ & - \int \overrightarrow{dX}\varphi^i[\beta\rho_r\overrightarrow{g} - \beta\bar{\Lambda}_r\overrightarrow{Gr}] - \int \overrightarrow{dX}\overrightarrow{\nabla}(\beta\varphi^i)Pr \\ & + \int \overrightarrow{dX}\overrightarrow{\nabla}\varphi^i[\beta\mu_T(\overrightarrow{\nabla}\overrightarrow{vr} + \overrightarrow{\nabla}^t\overrightarrow{vr})] + BC \end{aligned} \tag{10}$$

with the same notations as above and $\bar{\Lambda}_r(Hr, \overrightarrow{Gr}, Pr)$ the total two-phase friction tensor, $\overrightarrow{vr}$=$\overrightarrow{Gr}/\rho_r$ and BC the boundary stress. The weakness concerning the non-linearity lies only in the values of μ_T, computed with the current iteration variables and not with the restricted ones.

5.1.5 The dynamic determination of the BC type (à la ADN)

The Adaptive Dirichlet Neumann (ADN) method, introduced by Quarteroni et al [15, 5, 16] is a particular domain decomposition method, not included in the zoom computation methods as previously described. But, the general strategy implied in the local BC determination can be fruitfully applied here. Roughly, the BC nature at a node of a given subdomain boundary is function of the sign of the dot product of the external normal and the fluid velocity. We set a Dirichlet condition at the inflow velocity nodes (negative sign) and a Neumann condition at the outflow velocity node (positive sign). Here, we follow this approach to face zoom computations with vortices located at interfaces. Dealing with a vortex at the interface is not really a problem for pure isothermal hydrodynamic computations, using the Chorin - Gresho algorithm. (It is to be noted that without any Neumann BC for the momentum balance equation, an ill-posed problem exists for the pressure.) Indeed, the problem comes with a reversal flow at the nodes of a fixed

Neumann BC interface for the energy balance equation. In this case, no value is supplied to the incoming specific enthalpy. To overcome this difficulty, we introduce the dynamic management of BC at outflow coupled boundaries.

The 'ADN' coupled surfaces are managed in the following way. At each coupling iteration:

1. Receive the mass flux field from the global domain (like a Dirichlet BC).
2. Eventually, apply a relaxation stage (see Eq. 4 and remark below).
3. Compute the dot product between the (eventually relaxed) mass flux and the outward normal. Determine the nature of the coupled BC by using the above rule. This holds for the momentum and the energy balance equations.
4. Compute again the matrix for the pressure equation (the BC nature has changed).
5. Receive the stress tensor field from the global domain (like a Neumann BC) and, eventually, apply a relaxation stage.
6. Receive specific enthalpy and thermal flux fields, with eventually relaxation.

At this point, some remarks are to be made.

Using relaxation stages leads to smoothing the changes of the BC values but may weaken the coherence between the mass flux fields of the zoom subdomain and the global domain.

Specific treatment is applied to the energy balance BC. The flow direction at the Neumann nodes of the 'ADN' coupled boundary may be inverted during the computation. In the case of inversions, we change the nature of the BC to the Dirichlet one, leading to freezing the enthalpy value to the last computed one. (This is released if the flow direction is inverted again.)

The previously presented strategy may be denoted as 'full ADN', because the mass flux and the specific enthalpy are concerned. It is possible to independently define the coupled BC for each balance equation, keeping the adaptive determination only for the energy one.

6 NUMERICAL TESTS

6.1 Test definition

For the SG simulation, we chose the CEA CLOTAIRE mock-up [17]. The riser part forms a half cylinder of 0.62 m in diameter and 9.16 m in height. The inside is filled with U-shaped tube bundle, 7.2 m in height, into which the hot primary flow enters. One flow distribution baffle, nine tube support plates and one anti-vibration bar are fixed in respectively the bottom, upright and curved part of the bundle. Our test cases are devoted to the zoom simulations of : (i) the U-tube bundle region above the last tube support plate, (ii) the flow distribution baffle region. In particular, we know of the existence of fluid vortices located in the U-tube bundle wake.

We compare the LDC zoom results (called LDC) with post-processing (or chained) Zoom computations, called Post. By post-processing, we mean a computation in two independent and successive steps: first, the computation of the global domain and, second, the computation of the zoom subdomain. We also compare the LDC zoom results with the global domain simulations at low and high space resolutions (respectively denoted Ref0 and Ref1).

In all the presented computations, the advection term is explicit. The physical models and the numerical parameters for the internal iterative method (here, Preconditioned Conjugated Gradient) are identical for all the simulations. In particular, the stationary criteria is $10^{-6}s^{-1}$ for the relative difference error per unit of time (with a maximum of 2,000 outer iterations).

We perform all the coupled simulations with two GENEPI tasks using a bi-processor computer (Sun Enterprise 2, model 2002, 200 MHz).

6.2 The CLOTAIRE U-tube bundle test case

6.2.1 LDC zoom and meshing

Concerning the global domain, we use two meshes. The first one, called the global coarse mesh, makes use of 5,330 cells. There are 780 hexahedral elements in the zoom region. The second one is called the global fine mesh (each cell of the coarse mesh is split into eight), see Fig. 2. This fine mesh is made of 42,640 cells. Fig.3 shows details of the meshes with the trace of the U-tube bundle. The mesh concerning the zoom subdomain is made of 6,240 cells (It is part of the global domain fine mesh). It is a slice of the riser with walls, inlet (bottom) and outlet (upper) areas, see Fig. 4.

6.2.2 Numerical features

The boundary conditions for the global domain computations are the usual ones. Concerning the zoom computations, there are specific boundary conditions for the exit (upper surface). Due to the presence of a vortex across this boundary, we use Adaptive Dirichlet Neumann (ADN) BC for the specific enthalpy and the mass flux. We also show results of computations with Dirichlet conditions for this boundary. For the LDC computations, the momentum and the energy balance equations on the global domain and on the zoom subdomain are coupled. Concerning the primary flow energy balance equation, the zoom inlet primary flow temperature and the zoom outlet thermal flux are coupled with the global domain (as in a domain decomposition method, DDM). The numerical parameters for the LDC computations are: coupling period $cp = 20$ outer iterations and relaxation parameter $\alpha = 1.0$ (unless explicitly stated). The number of corrected nodes in the global computation is 750 (but we have made computations with different numbers of corrected nodes).

6.2.3 Results

The performances concerning the CPU time (up to a relative difference per unit of time of about $5.10^{-3}s^{-1}$) and the memory are listed in Table 1. We can make some comments. The memory used in the LDC case and Chained case is similar (factor 2). They deeply differ from the memory needed in the case of Ref1 (factor 7). It is the same for the CPU time comparison. Moreover, with parallel computations, the LDC method leads to lower CPU time. Hence, it is possible to locally increase the accuracy of the computation (see below) on the global domain without increasing the cost too much. Concerning the CPU time spent for the coupling, the LDC iterations on the global domain or the updates of the boundary condition on the zoom domain cost about 10% of total CPU time. This ratio may be lower with an increase in mesh cell number.

Fig. 5 plots the convergence history of the mass flux variable for the reference global domain computation (Ref0, standard computation) and the LDC ones, using various BC natures (Dirichlet or ADN). All the convergence histories for the variables ($\vec{G}$, P, H, T_p) are given in terms of relative difference, between two consecutive outer iterations, in discrete L2 norm : $\Delta_r u$,

$$\Delta_r u = \frac{|u_n - u_{n-1}|_{L2}}{|u_{n-1}|_{L2}} = \frac{(\sum_{i=1}^{nd} |u_n^i - u_{n-1}^i|^2)^{0.5}}{(\sum_{i=1}^{nd} |u_{n-1}^i|^2)^{0.5}} \tag{11}$$

In Eq. 11, u stands for a variable, n for the outer iteration counter and nd for the number of nodes. Up to a relative difference of the order of 10^{-6}, the convergence histories are similar. Typically, after 10-15 LDC iterations (or about 200-300 outer iterations), the correction values are stabilized. In Fig. 6, we plot the evolutions of the relative correction terms for the mixture energy balance equation (mgc_H, see Eq. 9) and for the mixture momentum balance equation (mgc_G, see Eq. 10). Here, the test involves 450 corrected nodes. The evolutions of the relative residuals are also given. The L2 norms of the plotted quantities are defined by $|r_n|_{L2}/|r_0|_{L2}$,

where r stands for a correction term or a residual and n for the outer iteration counter.

Hence, the convergence of the LDC algorithm is fast. At the end of the computation, the discrete L2 norm of the energy correction is of a few kW. To compare, the exchanged power in the U-tube bundle region is of about 70 kW. Fig. 7 plots the convergence history of the zoom subdomain variables in case of computation with Dirichlet BC on the upper boundary. The convergence histories are similar to the ADN boundary case. Clearly, the computation convergence is significantly affected by the refreshments of the coupled boundary values at the beginning of the computation. In fact, the goal of the relaxation parameter α (here 0.5) is to partly damp these oscillations (a lower value does not greatly increase the damping). Some additional tests showed that the decrease of the coupling period (for instance, $cp = 5$) leads to a better convergence history with identical physical results. However, the coupling CPU time is increased : about 30% of the total CPU time in the case of $cp = 5$ instead of 10% in the case of $cp = 20$.

Fig. 8 shows the LDC fields on the coarse mesh computation for, respectively, the energy equation and the momentum equation (cut 5 cm inside the mock-up, detail of the global mesh). The energy correction terms are located at the border of the U-tube bundle and the momentum correction terms outside the anti-vibrating bars, see Fig.3.

Sequential computations were performed for the same test case ($cp = 20$), see Fig. 9. The results are similar. However, the convergence history is slightly smoother for the sequential case than for the parallel one. But obviously the CPU time is largely increased (factor two). In particular, we have also reported a convergence history for a computation with a coupling period of 100 outer iterations. No convergence acceleration is gained and the CPU time is higher. In fact, to solve the fine and coarse mesh systems at each coupling iteration is not a good strategy due to the strong non-linearities.

6.2.4 Physical features

Concerning some global quantities, such as the exchanged thermal power, the steam mass flow rate, ..., all the computations give similar results. For instance, the exchanged thermal power, in the LDC computation, is slightly overestimated (about 0.4% in comparison with the Ref1 case). In fact, the improvement due to by the LDC method is to be found in the local variation of the variables in the global domain. In particular, the isovalues of the specific enthalpy inside the correction region are closer to the Ref1 results than the Ref0 ones, even if some underestimations appear. In Fig. 10, we show the enthalpy distribution along one vertical line in the cold leg for the coarse and fine mesh computations alone (called coarse and fine) and for the LDC computation (called zoom and LDC coarse). The zoom extension is drawn with dashed vertical lines. The enthalpy profiles computed with the LDC on zoom or global domain are very close to each other and present the same variations as the Ref1 results. Obviously, the better the coarse grid results in the entry of the zoom, the better the zoom predictions.

6.2.5 Dynamic BC features

As previously stated, there is a vortex on the zoom upper boundary. We report in Fig. 11 the inflow node number history concerning this coupled boundary. This number quickly converges to 32 inflow nodes (about 25 coupling iterations). The inflow region coherency (between the local fine mesh zoom and the global coarse mesh riser) is satisfactory in regard of Fig. 12 and 13. In these figures, the inflow region (negative value of the dot product of the mass flux and the outward normal) is dark.

6.3 The CLOTAIRE flow distribution baffle test case

We briefly report results concerning the flow distribution baffle zoom computation. The function of this device is to force the flow to move toward the inner region. The particularity is an embedded zoom computation : the zoom boundary does not cross the global domain boundary.

6.3.1 Meshing

Fig. 14 shows a section of the global domain mesh (coarse) and of the zoom subdomain (fine). Fig.15 shows the fine mesh zoom with the flow distribution baffle (lower) and two support plates. This mesh is made of 2,048 cells. The coarse global domain mesh is the same as before.

6.3.2 Numerical features

The boundary conditions for the zoom computation are Dirichlet, except on the upper boundary (global outflow area) where those of adaptive BC are used ('à la ADN'). With regards to the flow distribution shown in Fig.15, the use of dynamic BC may seem needless : no vortex on the boundary. Neumann BC seems to be the right choice. In fact, the pressure distribution computed during the transient may lead to flow inversions... The momentum, the energy and the primary flow energy balance equations are coupled in the same way as before. The coupling period *cp* is 20 outer iterations and no relaxation stage is applied. The number of corrected nodes in the global computation is 147. These nodes are located between the flow distribution baffle and the first support plate, see Fig.15.

6.3.3 Results

Again, the convergence history is good and a fast convergence of the LDC values is achieved (after about 25 coupling iterations). Fig. 16 plots the convergence history of the zoom subdomain variables. The stationary criteria is reached at the outer iteration number 1,860. We can notice

a more perturbed period on the first 300 outer iterations. This is due to the time needed to set up the flow regime. During this period, a flow reversal is produced, see Fig. 17, but the adaptive BC used prevents the computation from failing. Finally, we present in Fig. 18 the isovalues of the vertical component of the mass flux in the zoom region. The left hand side picture is relative to the standard coarse mesh global computation (no LDC), the middle one to LDC coarse mesh global computation and the right one to the fine mesh Zoom. Again, the LDC prediction on the coarse mesh is close to the prediction on the fine mesh zoom in the corrected region (between the flow distribution baffle and the first support plate).

7 CONCLUSION

We have proved the efficiency of an additive version of a zooming algorithm based on the LDC method in the simulation of Steam Generator two-phase flows. The possibility of a local adaptive zooming for flow simulation around obstacles and a locally improved description for the global Steam Generator domain have been achieved. In particular, this original approach applies, for non-linear equations, a parallel version (instead of sequential) of the LDC Method, without solving the balance equations, but only using a few iterations of an iterative process. The LDC computation allows the enhancement of the software prediction in the correction region: (i) the behaviour of the variables is between the result of the computations with coarse and fine mesh, (ii) the coherence between the zoom subdomain results and those of the global domain is enhanced. The LDC computation cost (zoom and global domains) is slightly higher than a post-chained computation and, obviously, much cheaper than the global domain one with the fine mesh. This work was completed with an adapted method, to face an eventual vortex presence at subdomain interfaces, suggested by the Adaptive Dirichlet Neumann method [5].

It consists in a first attempt to bring modern numerical tools into the context of industrial

simulations of SG two-phase flows. In the zoom computation framework, future improvements are planned. In particular, we can mention the development of a version of the Flux Interface Correction method (FIC) [18, 19]. We plan to improve the flux coherence at the coupled boundaries. We must outline the interest of the code-linker (like that of the CEA, ISAS) to parallelize tasks using a network, without code re-engineering. However, this choice involves limitations on parallel computation capacities.Moreover, the implementation is versatile enough to be extended to Domain Decomposition Methods [13], to equation coupling or to multigrid preconditioning such as the Full Approximation Storage (FAS) method ([20], development under progress).

Acknowledgments

We would like to thank the Framatome Company for its financial support.

References

[1] W. Hackbusch. *Local Defect Correction Method and Domain Decomposition Techniques*, volume 5 of *Computing Suppl.*, pages 89–113. Springer-Verlag (Wien), 1984.

[2] M. Grandotto, M. Bernard, J.P. Gaillard, J.L. Cheissoux, and E. De Langre. A 3D finite element analysis for solving two phase flow problems in PWR steam generators. In *7th International Conference on Finite Element Methods in Flow Problems*, Huntsville, Alabama, USA, November 1989.

[3] M. Grandotto and P. Obry. Calculs des écoulements diphasiques dans les échangeurs par une méthode aux éléments finis. *Revue Européenne des Eléments Finis*, 5(1):53–74, 1996.

[4] P. Obry, J.L. Cheissoux, M. Grandotto, J.P. Gaillard, E. De Langre, and M. Bernard. An advanced steam generators design 3D code. In *ASME Winter Annual Meeting*, Dallas, Texas, USA, November 1990.

[5] A. Quarteroni. Domain decomposition method for the numerical solution of partial differential equations. Technical Report UMSI90/246, Supercomputer Institute, University of Minnesota, 1990.

[6] E.D. Hughes and F.T.W. Chen. Transient three dimensional thermalhydraulic analysis of homogeneous two phase flows in heat exchangers. In *AICHE National Heat Transfer Conference, PWR Steam Generators*, 1977.

[7] H. Schlichting. *Boundary Layer Theory.* Mac Graw Hill, 1968.

[8] G. S. Lellouche and B. A. Zolotar. Mechanistic Model For Predicting Two-Phase Void Fraction For Water in Vertical Tubes, Channels, and Rod Bundles. EPRI Report NP 2246-SR Special Report, 1982.

[9] N. Zuber and J.A. Findlay. Average Volumetric Concentration in Two-Phase Flow Systems. *J. Heat Transfert*, 87:453–468, 1965.

[10] P.M. Gresho and S.J. Chan. On the theory of semi implicit projection methods for viscous incompressible flow and its implementation via finite element method that also introduces a nearly consistent matrix. i, theory. *International Journal for Numerical Methods in Fluids*, 11(5):587–620, 1990.

[11] P.M. Gresho, R. Lee, and R. Sani. Advection-Dominated Flows with Emphasis on the Consequences of Mass Lumping. *Finite Elements in Fluids*, 3:335–350, 1978.

[12] P.M. Gresho, R. Chan, S.J. Lee, and C. Upson. A modified finite element method for solving the time dependent, incompressible Navier Stokes equations (Part 1: Theory). *Int. J. Num. Methods in Fluids*, 4:557–598, 1984.

[13] M. Belliard and M. Grandotto. Two-phase fluid flow computation in steam generator using a domain decomposition method. In *Computational Fluid Dynamics98, Proceeding of the Fourth European Fluid Dynamics Conference*, volume 1, pages 186–191, Athens, Greece, September 1998. Wiley.

[14] Th. De Gramont and I. Toumi. ISAS user's guide. Technical Report SERMA/LETR/96/1955, CEA, Saclay, France, 1996.

[15] C. Carlenzoli and A. Quarteroni. Adaptive domain decomposition methods for advection-diffusion problems. In Babuska I. e. a. (ed) Modeling, Mesh Generation and Adaptive Numerical Methods for Partial Differential Equations, volume 75 of IMA Volumes in Mathematics and its Applications, pages 165-199, Springer verlag edition, 1995.

[16] L. Gastaldi, F. Gastaldi and A. Quarteroni. ADN and ARN domain decomposition methods for advection-diffusion equations. Ninth International Conference on Domain Decomposition Methods, Editor Petter Bjorstad, Magne S. Espedal and David E. Keyes., 1998.

[17] J.L. Campan and J.C. Bouchter. Steam generator experiment for advanced computer code qualification : CLOTAIRE international program. In *Third International Topical Meeting on nuclear power plant thermohydraulics and operations*, Seoul, April 1988.

[18] Ph. Angot, J. P. Caltagirone, and K. Khadra. Une méthode adaptative de raffinement local: la correction du flux à l'interface. *C. R. Acad. Sci. Paris, Sér. I*, 315:739–745, 1992.

[19] Ph. Angot, J. P. Caltagirone, and K. Khadra. A comparison of locally adaptive multigrid methods: L.D.C., F.A.C. and F.I.C. In *NASA Conf. Publ.CP-3224*, volume 1, pages 275–292, 1993.

[20] A. Brandt. Multi-level adaptive solutions to boundary-value problems. *Mathematics of Computation*, 31(138):333–390, 1977.

Tables

Simulation	iterat. ♯	CPU (s)	Memory (Mo)
Ref0	493	1960	20
Ref1	1079	27820	280
Chained ◇	371	2950	40
LDC global	520	2270	40
LDC zoom	520	3270	80

◇ Requires Ref0 as first stage

Table 1: Efficiency of the // LDC zoom computation.

Figure captions

List of Figures

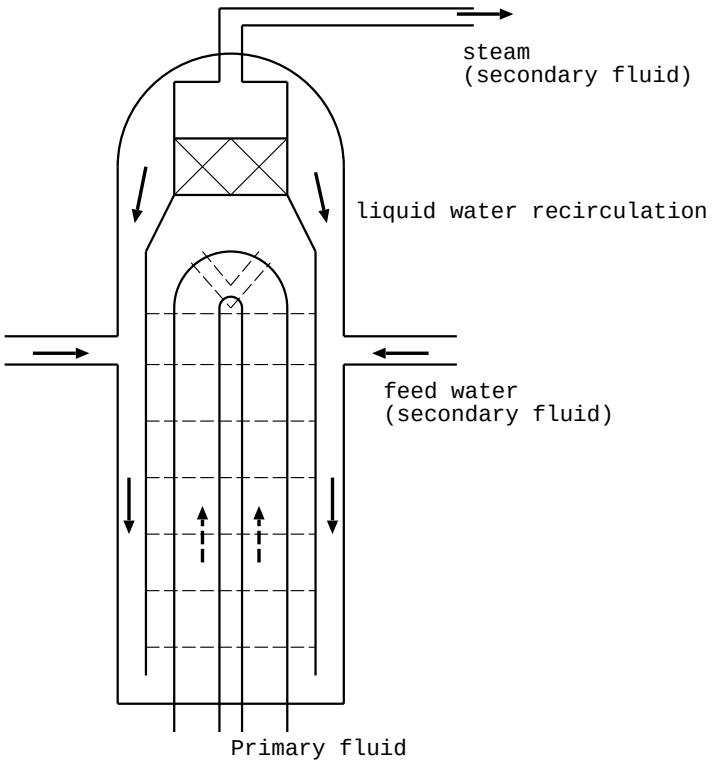

Figure 1: French nuclear steam generator (diagram)

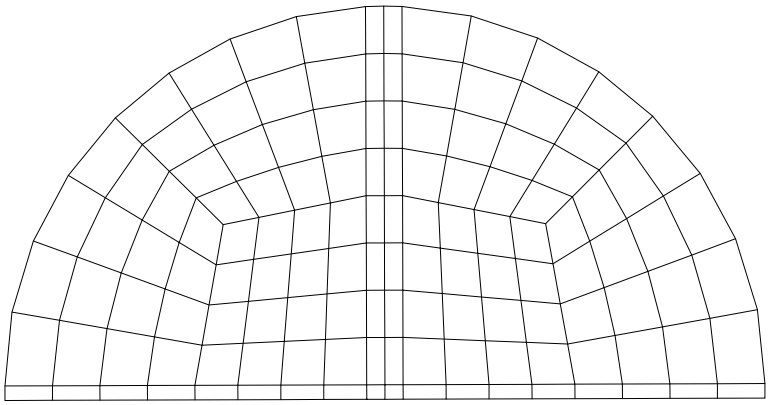

130 cells

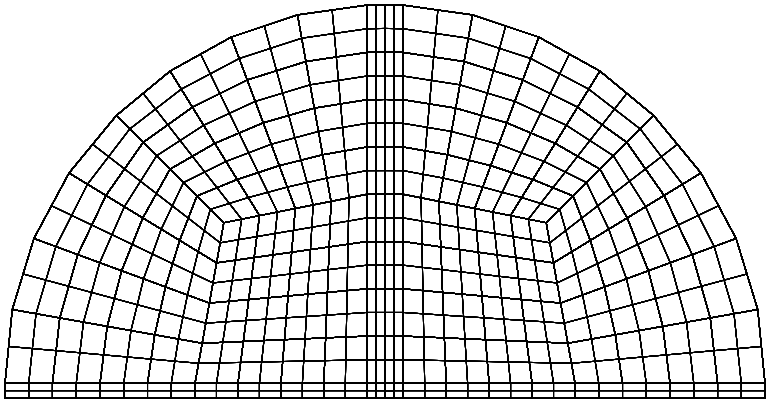

520 cells

Figure 2: Coarse and fine meshes (2D sections of the 3D meshes). Top: coarse mesh (130 x 41 = 5,330 cells), bottom: fine mesh (520 x 82 = 42,640 cells).

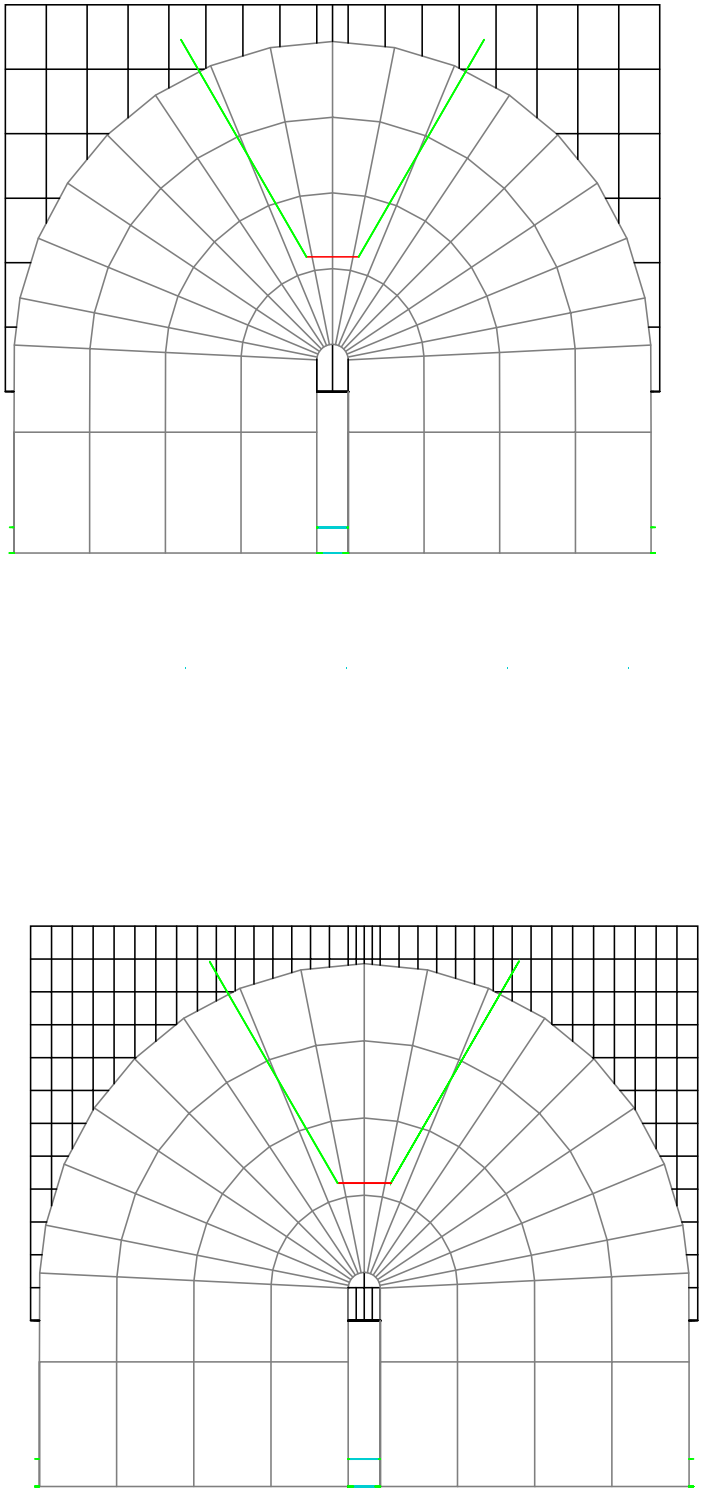

Figure 3: Meshes and U-tube bundles (detail); 2D side view. Top: partial coarse mesh (130 x 6 = 780 cells), bottom: partial fine mesh (520 x 12 = 6,240 cells).

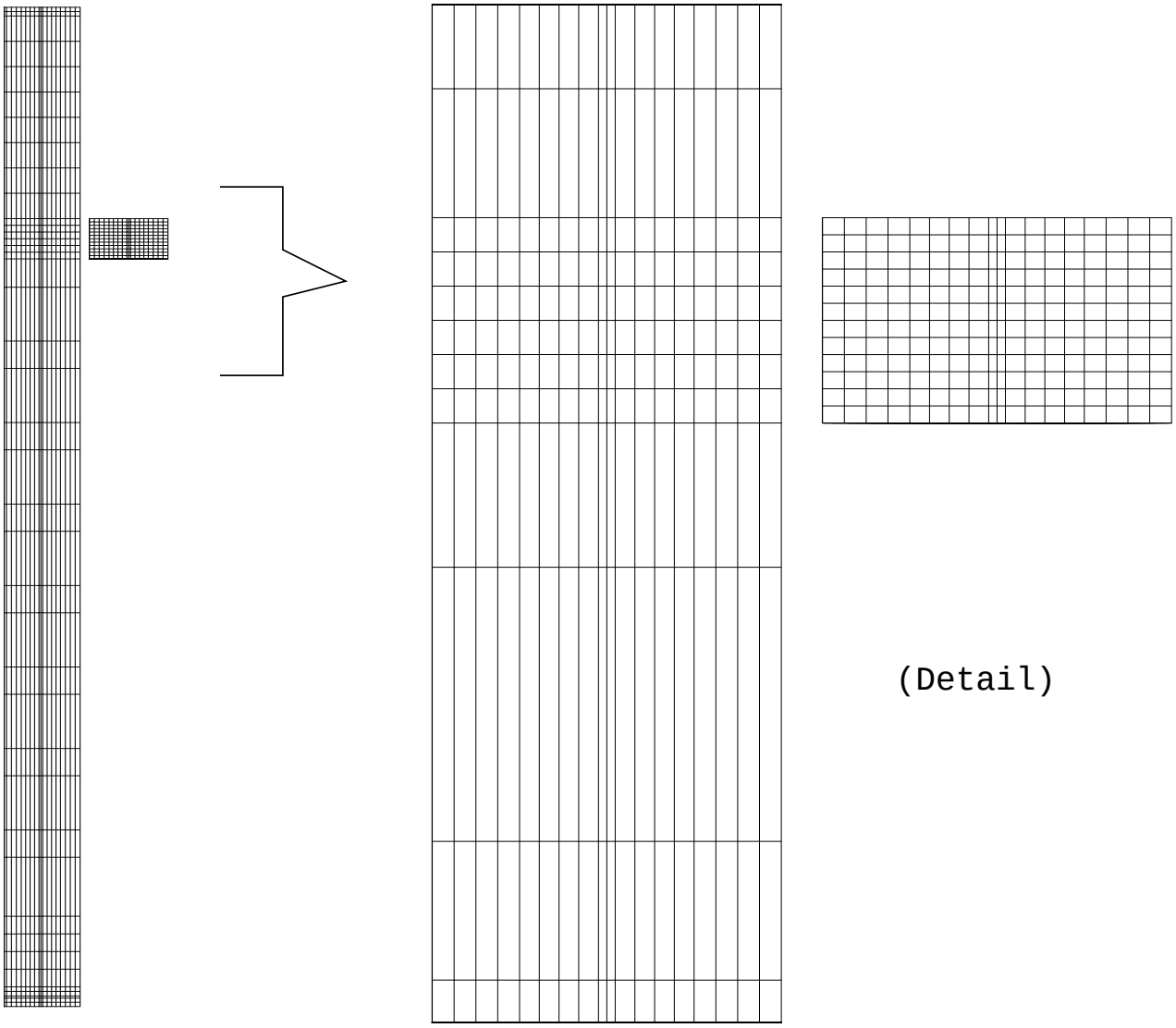

Figure 4: Coarse and fine meshes for the zoom region (2D side view).

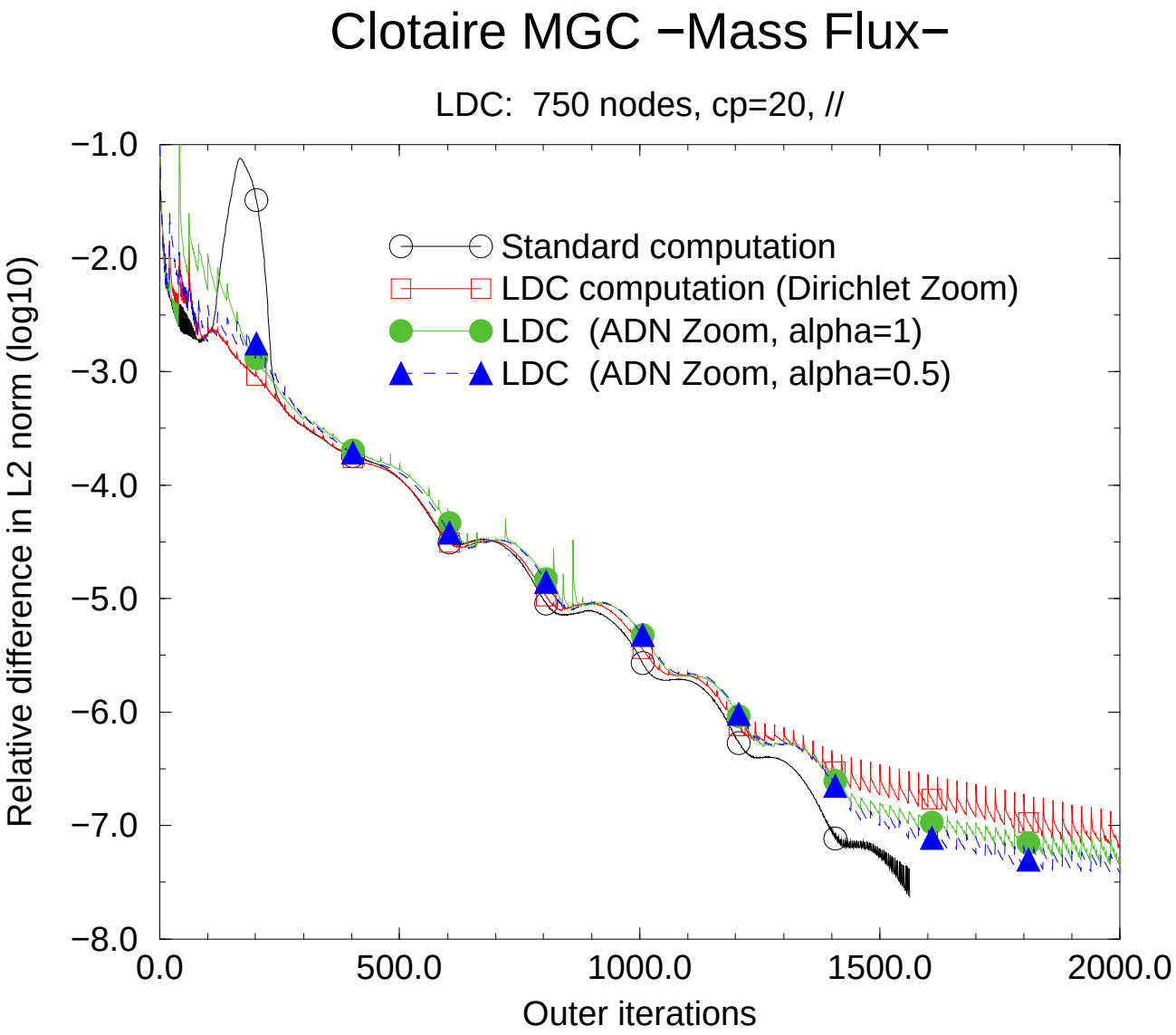

Figure 5: Mass flux convergence history, global domain

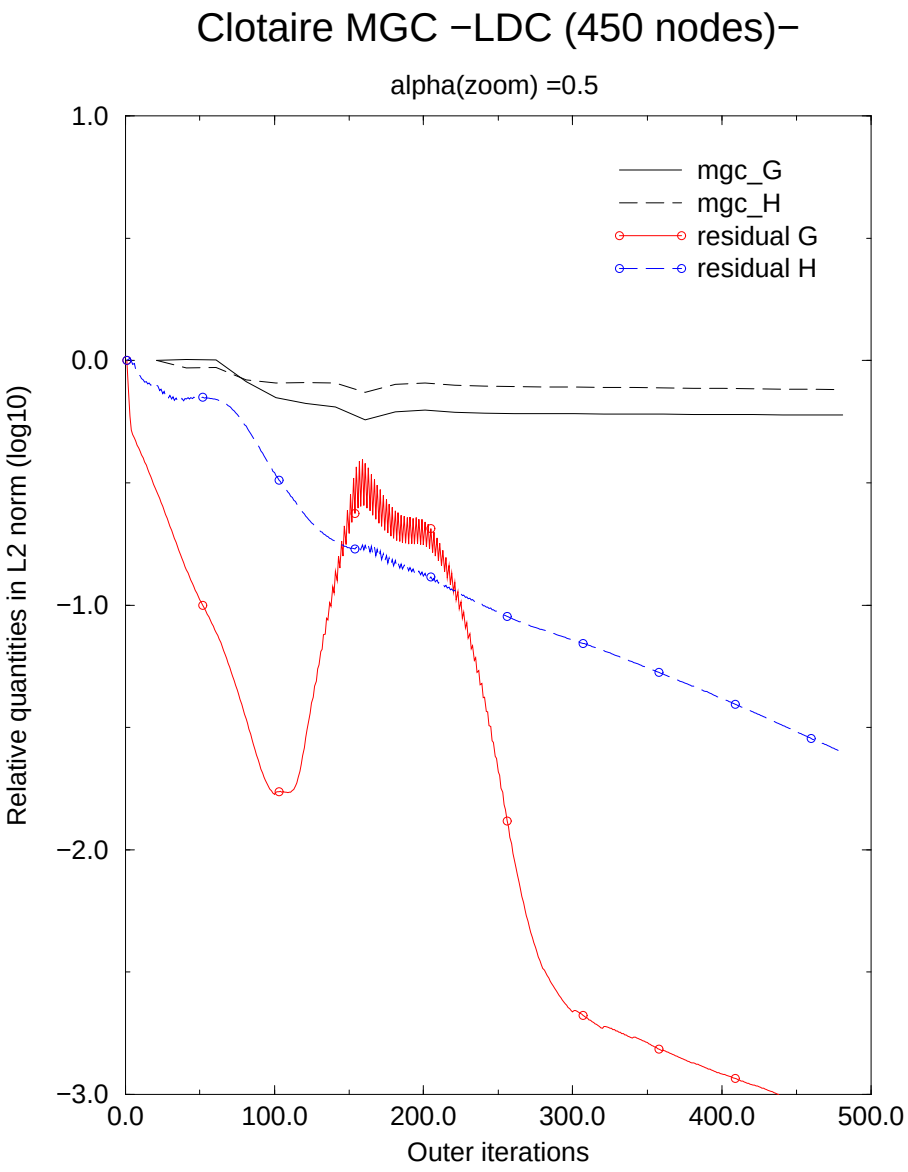

Figure 6: Residual and LDC convergence history, global domain

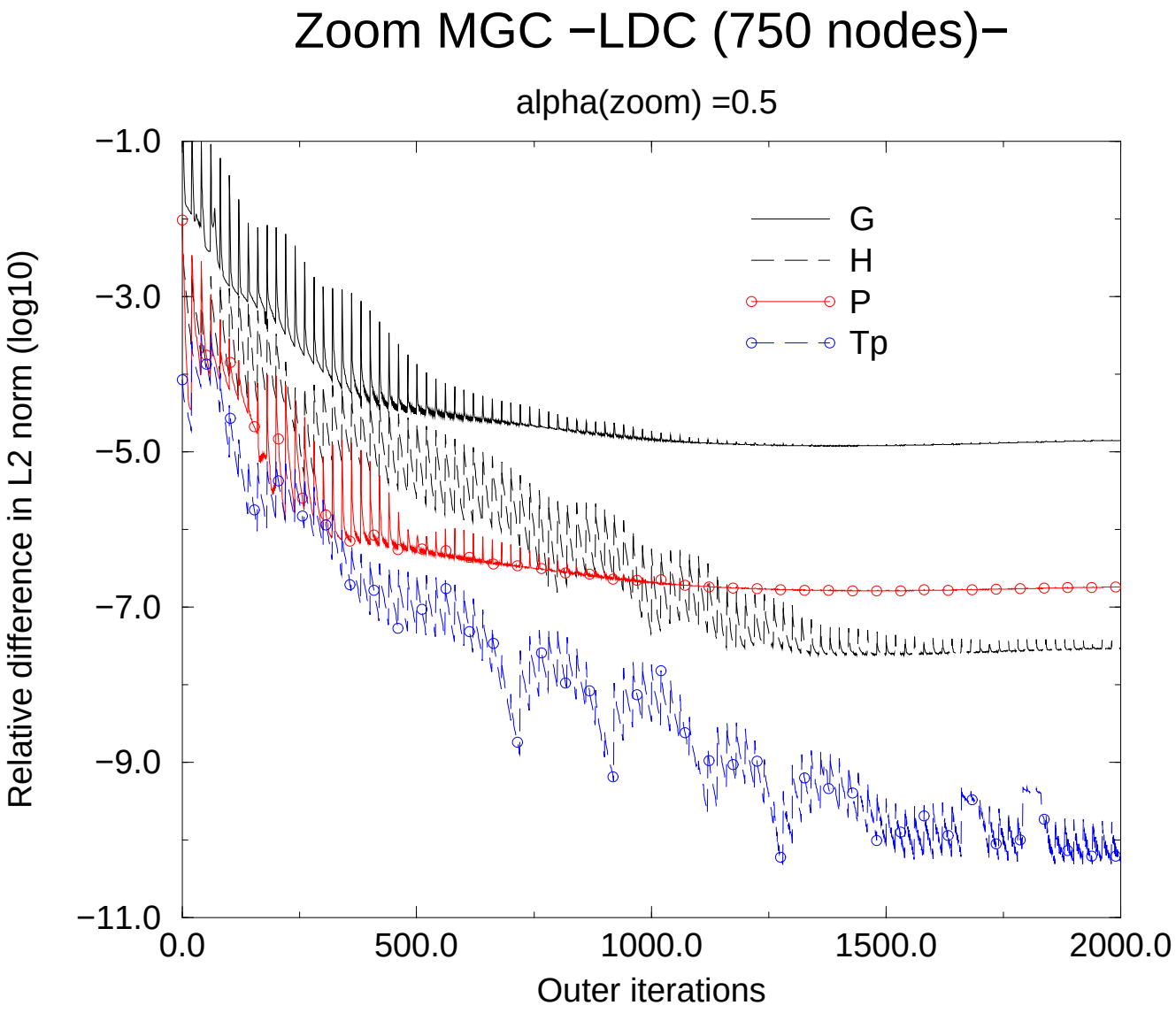

Figure 7: Variable convergence history, zoom domain

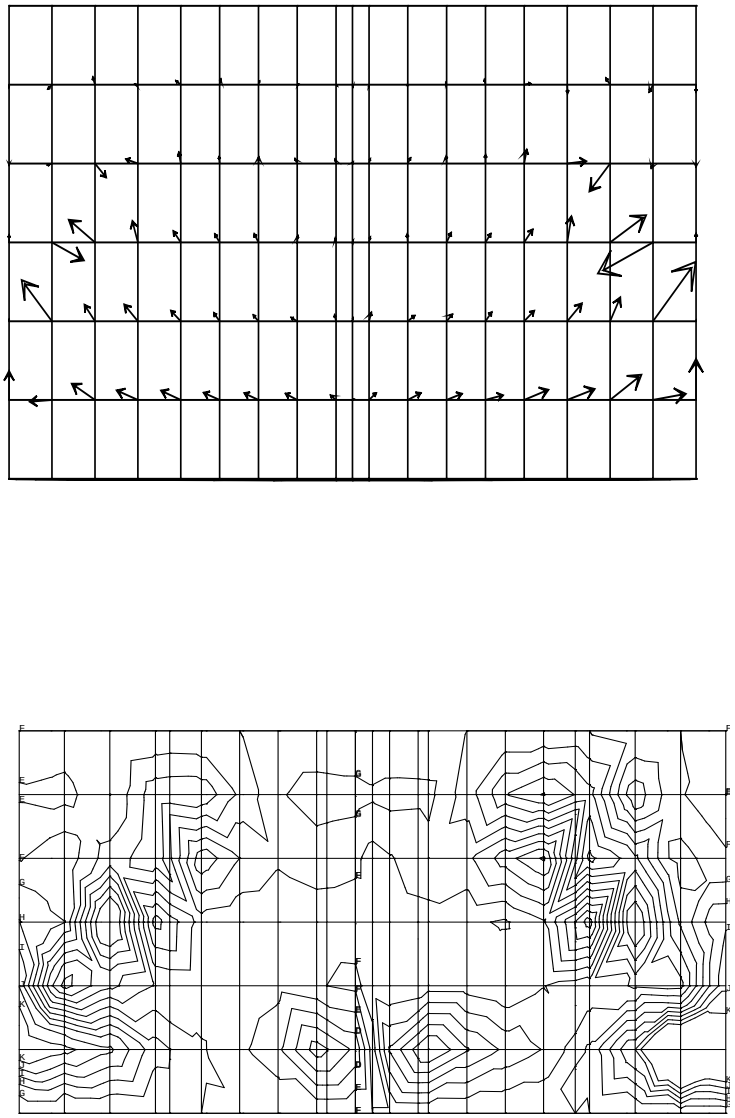

Figure 8: Correcting term fields (top: energy balance equ., bottom: momentum balance equ.). Momentum balance equ.: typical vector length: 1 N; Energy balance equ.: step between isocontours is 200 W; min.: -1020 W; max.: 1300 W.

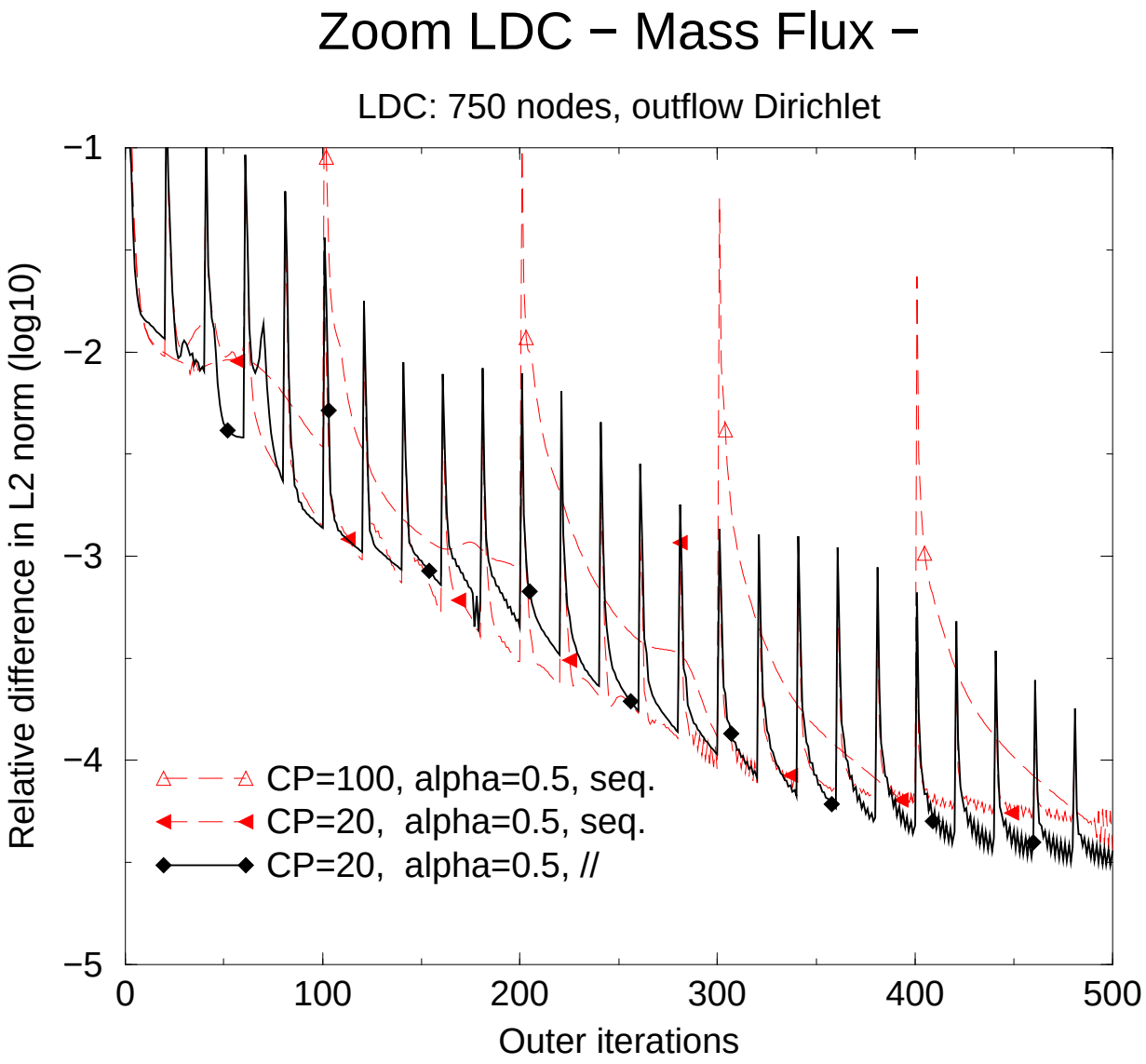

Figure 9: Multiplicative (seq.) and additive (//) algorithm

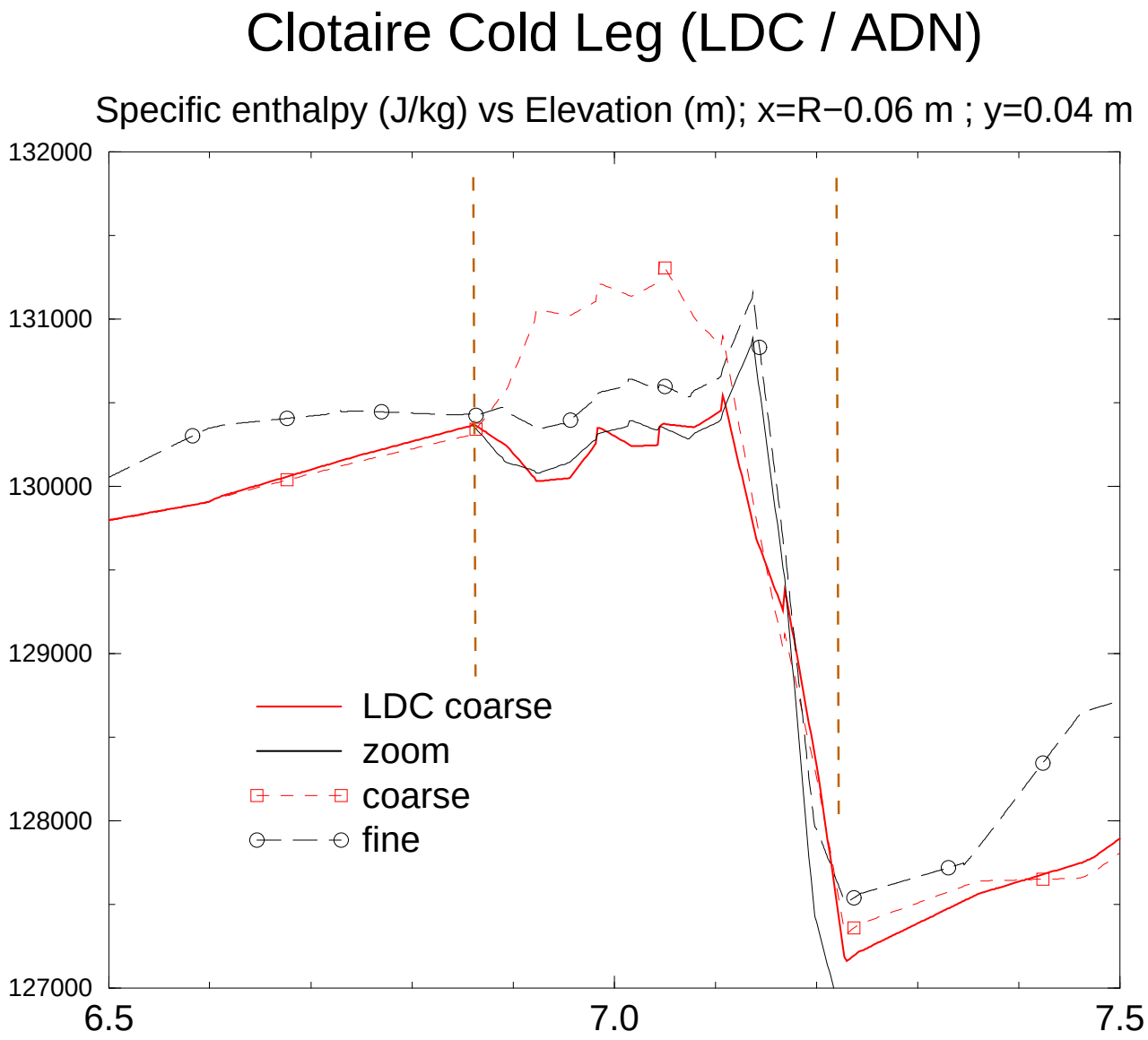

Figure 10: Specific enthalpy in cold leg

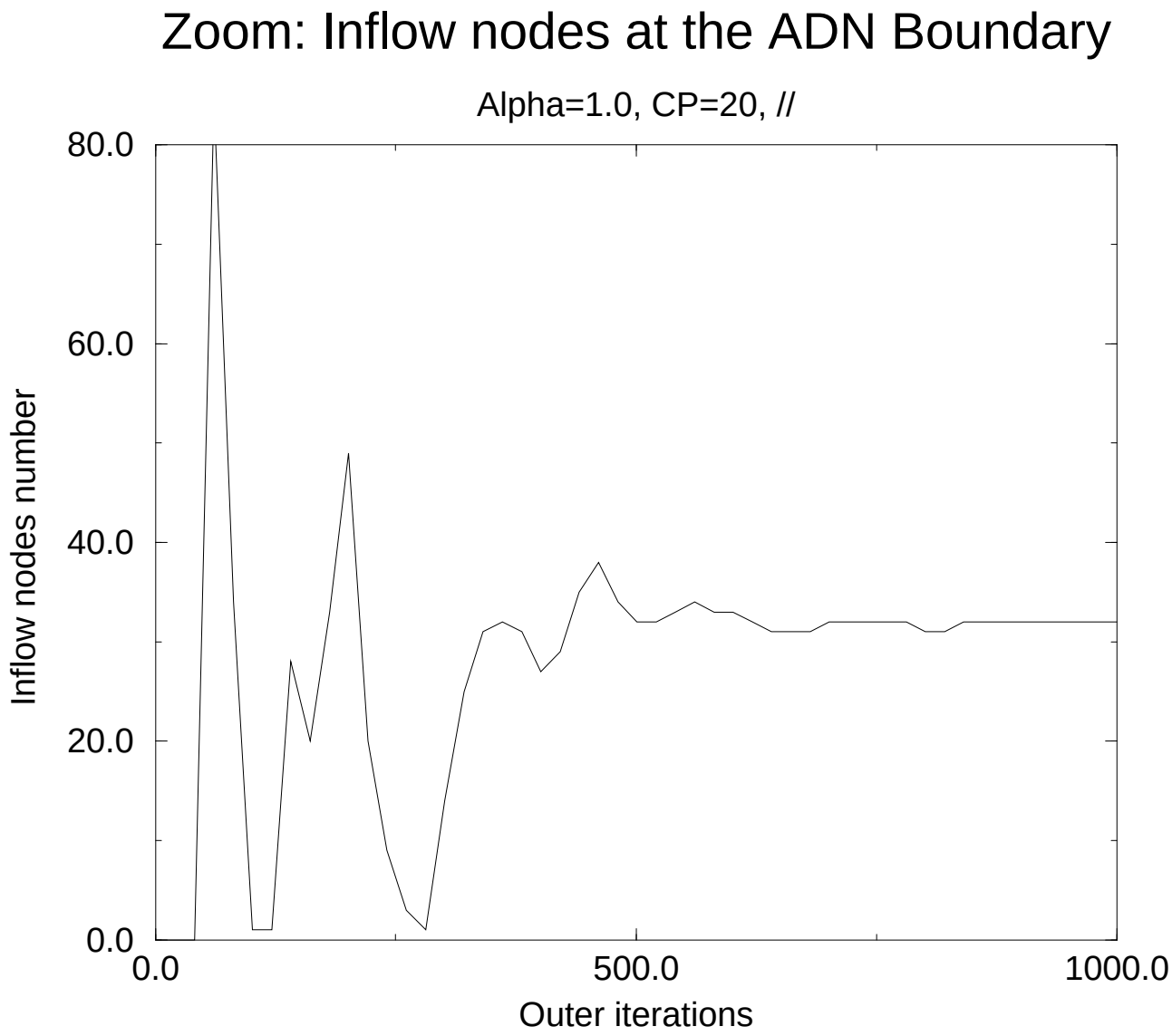

Figure 11: Zoom sub-domain inflow

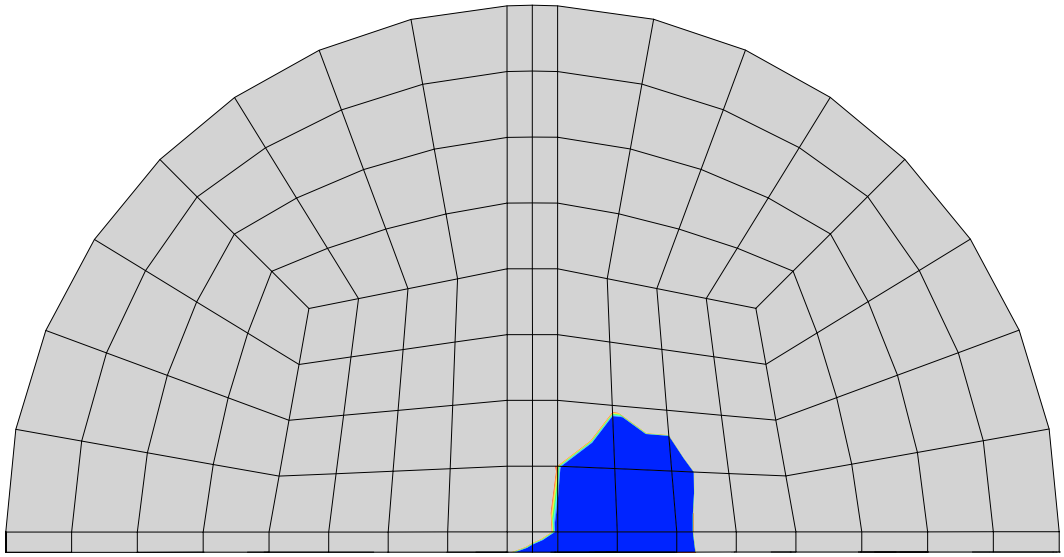

Figure 12: Coarse mesh riser section at the elevation of the fine mesh zoom upper interface

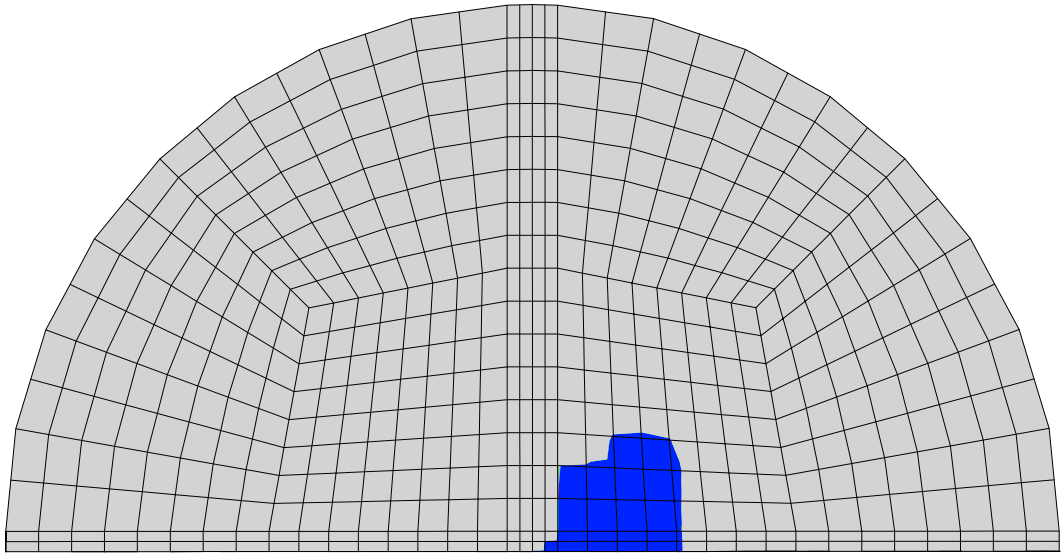

Figure 13: Fine mesh zoom upper interface

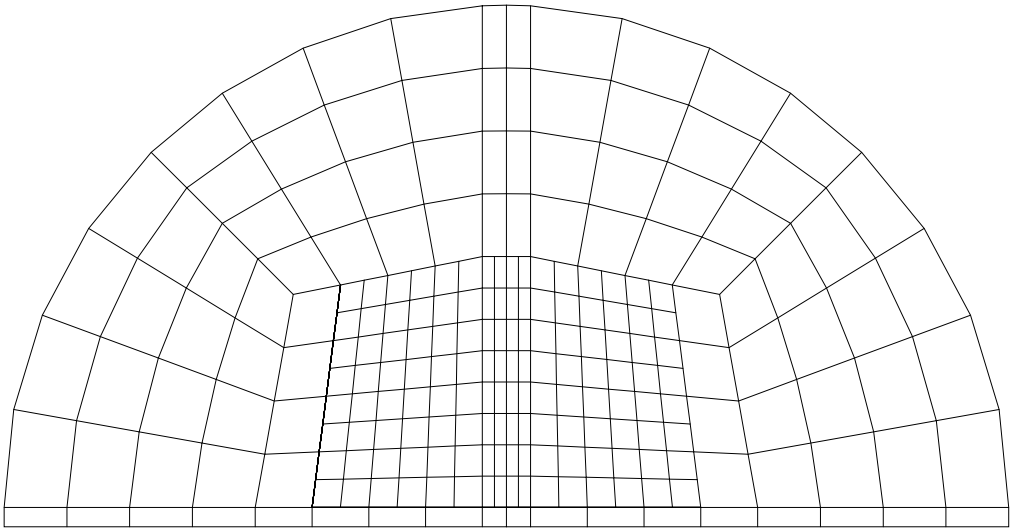

Figure 14: Embedded zoom computation mesh (section)

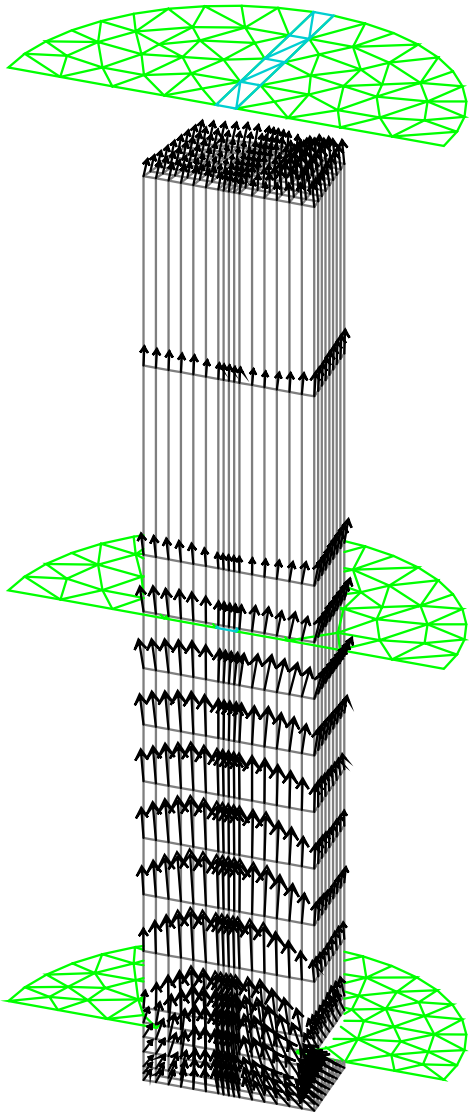

Figure 15: Embedded zoom computation mesh

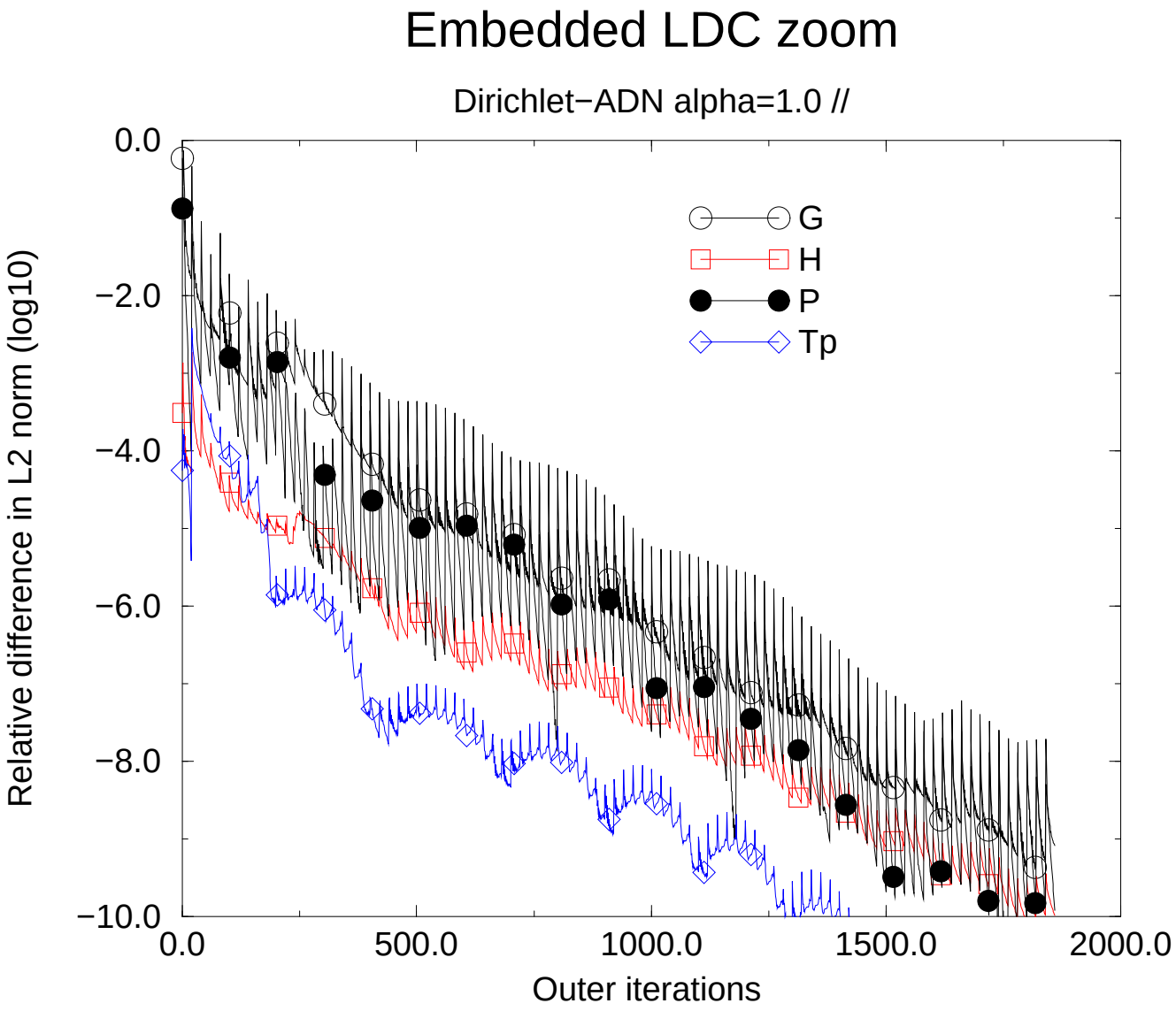

Figure 16: Zoom convergence history (embedded zoom)

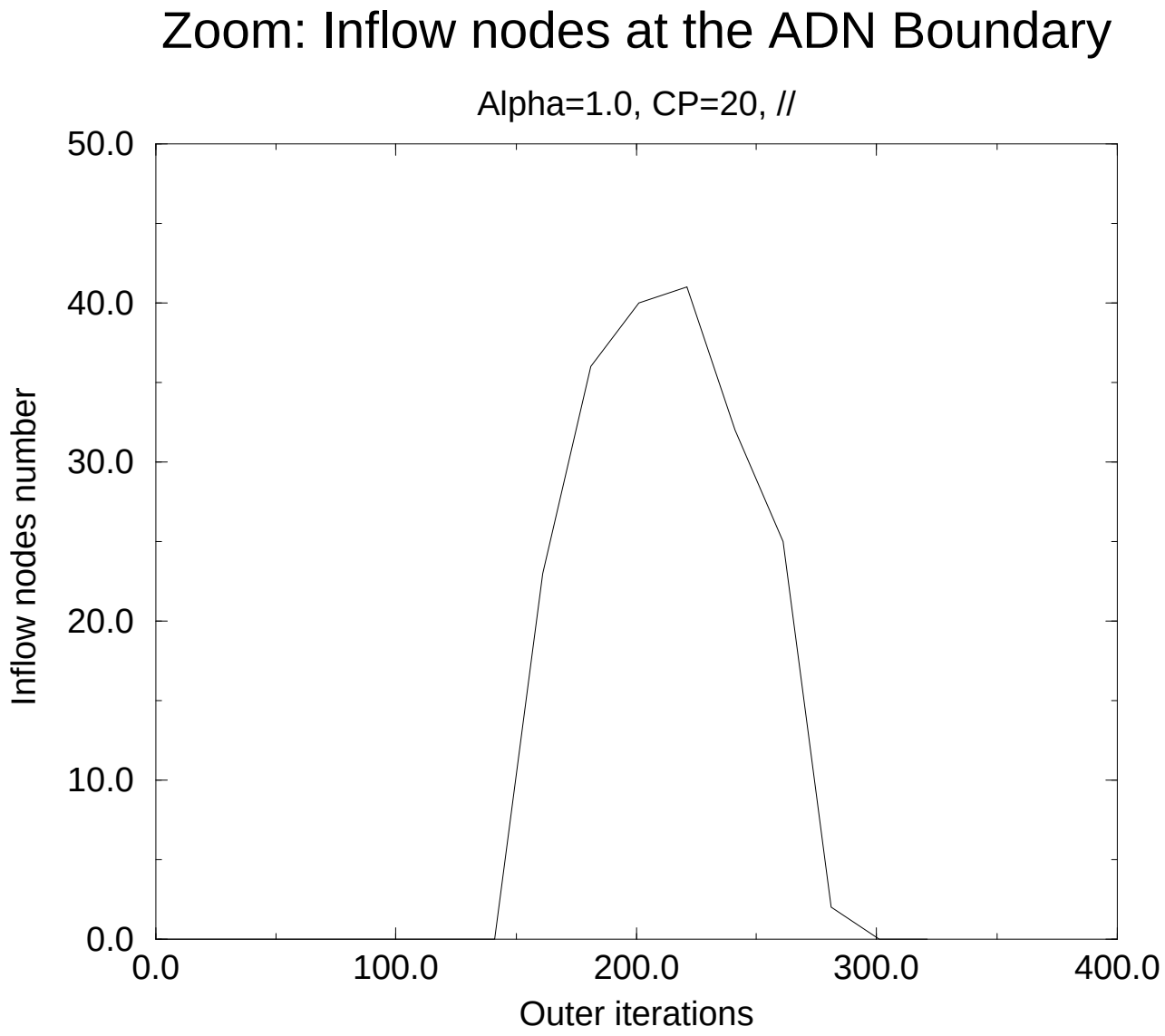

Figure 17: Zoom sub-domain inflow (embedded zoom)

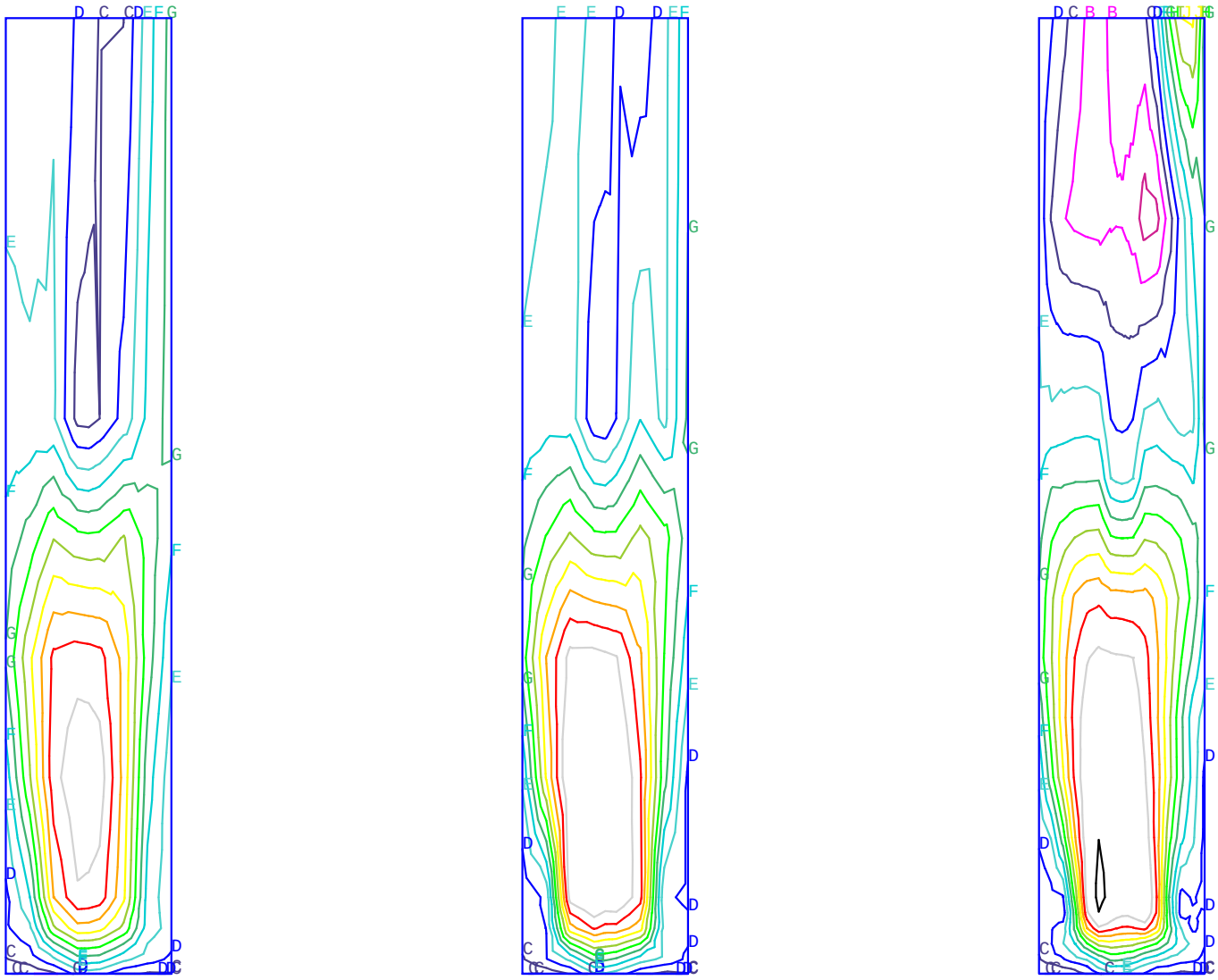

Figure 18: Vertical mass flux (embedded zoom) - Left: coarse mesh (standard), Middle: coarse mesh (LDC 750 nodes), Right: fine mesh Zoom - Step between isocontours is 68 kg/m2/s; min.: 244 kg/m2/s; max.: 1260 kg/m2/s